**Natural Hazards
and Earth System
Sciences**
Open Access

Discussions

Real-scale investigation of the kinematic response of a rockfall protection embankment

S. Lambert[1], A. Heymann[1,2,3], P. Gotteland[2], and F. Nicot[1]

[1]Irstea, UR ETGR, 2 rue de la papeterie, 38402 St-Martin d'Hères, France
[2]3SR, UJF-INPG-CNRS-UMR5521, DU Grenoble Universités, 38041, currently, FNTP, 3 rue de Berri, 75008 Paris, France
[3]Razel Society, Groupe Fayat, 3 rue René Razel, Christ de Saclay, 91892 Orsay Cedex, France

Correspondence to: S. Lambert (stephane.lambert@irstea.fr)

NHESSD

2, 491–533, 2014

Real-scale response of a protection embankment

S. Lambert et al.

Title Page

Abstract	Introduction
Conclusions	References
Tables	Figures

|◀ | ▶|
◀ | ▶
Back | Close

Full Screen / Esc

Printer-friendly Version

Interactive Discussion

Abstract

This paper addresses the response of rockfall protection embankments when exposed to a rock impact. For this purpose, real-scale impact experiments were conducted with impact energies ranging from 200 to 2200 kJ. The structure was composed of a 4 m-
[5] high cellular wall leaned against a levee. The wall was a double-layer sandwich made from gabion cages filled with either stones or a sand–scrapped tyre mixture. For the first time, sensors were placed in different locations within the structure to measure real-time accelerations and displacements. The test conditions, measurement methods and results are presented in detail. The structure's response is discussed in a descriptive
[10] and phenomenological approach and compared with previous real-scale experiments on other types of embankments.

1 Introduction

Land constraints due to increasing urbanization and economic growth of mountainous areas have motivated the development of different types of protection structures
[15] against natural hazards such as snow avalanches, rockfall and debris flows. Among these structures, embankments aim at protecting areas exposed to frequent occurrence and high-energy rockfall. Classically, these structures consist of reinforced earth dams, associated with a ditch for containing the intercepted blocks (Peila, 2011; Lambert and Bourrier, 2013). These structures exhibit a quasi-vertical mountain-side facing
[20] to prevent the ramp effect. The economic considerations in natural hazard management warrant significant research to improve the efficiency of these structures in terms of both their ability to withstand the impact and their efficiency in halting blocks (Lambert et al., 2013).

Many studies have been conducted with the aim of investigating the mechanical
[25] response of embankments for optimisation purposes (Peila, 2011; Lambert and Bourrier, 2013). In particular, real-scale experiments on embankments with impact ener-

gies higher than 1000 kJ have been conducted by different authors (Burroughs et al., 1993; Hearn et al., 1995, 1996; Yoshida, 1999; Peila et al., 2000, 2007; Maegawa et al., 2011). Impact experiments on real-scale structures have also investigated lower-energy rockfall (Aminata et al., 2008; Sung et al., 2008). In parallel, the cost of such experiments has motivated small-scale experiments in view of parametric studies (Blovsky, 2002; Hofmann et al., 2013). These studies have provided qualitative results of great value, but from a quantitative point of view questions concerning the similarity of these experiments may arise, in particular for 1 g tests.

The structures concerned by the real-scale experiments differ in shape, construction materials and size. For obvious cost reasons, the number of tests for each is rather limited. Extrapolation to other structures and to higher block kinetic energies may not be straightforward. Moreover, these studies provided only few experimental data with respect to the response of the structure over time. Indeed, apart from data related to the block trajectory, measurements mainly concerned the embankment surficial deformation after impact.

This paper focuses on the mechanical response over time of composite protection embankments made of geocells. The use of geocells associating a manufactured envelope with a fill geo-material was first proposed by Yoshida (Yoshida, 1999) for building rockfall protection embankments. The main advantage of such composite structures compared to monolithic and rigid ones is that they allow the impact energy to be transformed into deformation energy, mainly in the cellular protection wall, avoiding deformation within the rest of the structure (e.g. ground compacted levee). It is also possible to adapt the mechanical characteristics of the geocell depending on its position in the structure by changing the fill material. Finally, the cellular nature of the structure facilitates its repair in case of severe damage after impact.

In this study, the choice was made to use two materials exhibiting very different mechanical characteristics: a sand–tyre shred mixture and crushed limestone. Gabion cages were considered as geocell envelopes to provide a vertical front for the structure facing exposed to impact, referred to as the front facing.

Title Page

Abstract | Introduction

Conclusions | References

Tables | Figures

◄ | ►

◄ | ►

Back | Close

Full Screen / Esc

Printer-friendly Version

Interactive Discussion

To develop the use of such cellular rockfall protection embankments, an extensive research study was initiated, combining experiments with numerical modelling and following a multi-scale approach, from the constitutive material to the structure scale. For instance, experimental and numerical studies at the geocell scale (Bertrand et al., 2005; Lambert et al., 2009, 2011) and at the scale of an assembly of geocells were conducted (Bourrier et al., 2011; Dimnet el al., 2013; Heymann et al., 2010, 2011). The experimental facet of this study placed an emphasis on measurement systems with the aim of providing data for both investigating the structure's response and validating the numerical models developed at the same time. In addition to the re-use of end-of-life tyres, pollution to the environment and fire risk issues were also addressed (Hennebert et al., 2014).

This paper presents the real-scale impact experiments conducted in this study and addresses the impact response of the embankment under different impact energies. A detailed description of this innovative structure is given together with the instrumentation involved. The test results are analysed focusing on the mechanical response of the structure subjected to a 210 kJ impact. The objective was to identify the kinematic response of the structure during the impact. Then the results from tests with impact energies up to 2200 kJ are presented. The discussion highlights the main features of the response of embankments to localized impact.

2 Materials and methods

2.1 Impacted structures

The tested structure consists of a two-layered cellular sandwich wall leaned against a ground-compacted levee (Fig. 1). The sandwich wall is 4 m high, 8 m long and 2 m thick. The geocells consist of gabion cages made up of a hexagonal wire mesh with an 80 mm × 120 mm mesh, and a 2.7 mm-diameter wire. Gabion cages are parallelepiped in shape, 3 m or 2 m long, subdivided into three or two 1 m^3 cubic parts, respectively.

Different fill granular materials are used according to the geocell location in the structure to form the layers of the sandwich. A crushed quarry limestone, 80–120 mm in grain size, is used for the front-facing geocells and a sand–shredded tyre mixture fills the kernel geocells. The sand size distribution ranges from 0 to 4 mm. The sand–tyre mixture contains 30 % by mass of tyre pieces with no particular shape with a size ranging from 20 to 150 mm. The tyre pieces result from the shredding of recycled end-of-life tyres. This material was considered both for waste recycling purposes and to take advantage of its particular mechanical characteristics: this mixture constitutes a reinforced composite material and is expected to attenuate dynamic loadings (Zornberg et al., 2004; Lee and Roh, 2007; Gotteland et al., 2008). A non-woven needle-punched geotextile is used to maintain this fine fill material within the gabion cage.

As is done on actual worksites, the empty gabion cages are positioned at their final place and stapled together (five to eight clips per edge). Stone geocells (i.e. geocells filled with crushed limestone) are filled with 0.30 m-thick layers of stones using a power-shovel; the facing stones are arranged by hand. Sand and scrapped tyres were mixed onsite before being poured into the geocell to form sand–tyre geocells (i.e. geocells filled with the sand–tyre mixture). Internal connecting wires are placed across both stone geocells and sand–tyre geocells every 0.30 m during filling to prevent geocell deformation as a result of gravity loading. This is also intended to facilitate repair work in case of severe damage to the front facing due to a block impact. Uncertainty associated with the gabion cage volume makes accurate geocell unit mass measurement impossible. From previous experiments in this study, an approximate unit mass of 1400 kg m^{-3} and 1600 kg m^{-3} can be considered for sand–tyre geocells and stone geocells, respectively.

The levee was made using ground materials on site, compacted by 0.5 m-thick layers with a vibrating-plate compactor, giving an average unit mass of 1970 kg m^{-3} (ranging from 1850 kg m^{-3} to 2100 kg m^{-3}). However, soil near the cellular sandwich wall was not compacted to avoid damaging the inclinometers in the levee (see Sect. 2.3).

Title Page

Abstract | Introduction

Conclusions | References

Tables | Figures

|◀ | ▶|

◀ | ▶

Back | Close

Full Screen / Esc

Printer-friendly Version

Interactive Discussion

2.2 Experimental equipment

The experiments were conducted in a limestone quarry in the French Alps. This site offers a 100 m-long pithead at the toe of a 30 m-high quasi-vertical cliff, for installing the conveying system and building the structure.

The conveying system is a cableway composed of a steel cable 50 mm in diameter anchored at the top of the cliff and beyond the structure location. The projectile is hung by a cable sling connected to a trolley placed on the cable. The trolley is then pulled up to the targeted position before being released. The trolley conveys the sphere downwards to the embankment, reproducing realistic impacts, that is (i) in a slanting direction with respect to the structure's front facing with angles ranging from 18° to 24° (ii) with a 28 m s^{-1} maximal impact velocity and (iii) at heights ranging from 1.75 m to 2.10 m from the natural ground. These characteristics can be considered representative of mean natural event characteristics.

For safety reasons and because of possible interaction with equipment used for quarrying operations, it was not possible to use pyrotechnic release systems as is often the case when testing rockfall protection structures. The projectile remains suspended to the pulley throughout the test. Controlling the projectile trajectory before the impact and the impact location is the advantage of this technical solution.

The projectile consists of two half-spheres made of steel, 20 mm thick, welded along the median plane to form a 1.60 m-diameter sphere. This sphere is filled with concrete giving the projectile a mass of 6500 kg. Its unit mass is approximately 3030 kg m^{-3}, which is considered satisfactorily close to the unit mass of rocks. An inside space is left so that accelerometers can be inserted at its mass centre. Even though the conic shape is more penetrative (Pichler et al., 2005), the spherical shape has been chosen because it facilitates interpreting the results to overcome issues related to the shape of the surface in contact with the structure during the impact. Phenomena that could result from the angular shape (punching or tearing the wire mesh) are avoided.

2.3 Measuring device

Different measuring techniques were employed to obtain data concerning the structure's response to impact. External measurements as well as internal measurements were taken, with the latter type concerning the projectile, the sandwich wall and the
5   levee. The majority are real-time measurements taken during the impact.

The instrumentation in the structure was designed considering the particularity of the context: (i) a structure partly built with coarse noncohesive granular material, (ii) existence of discontinuities (gabion cages) and (iii) large and localized deformation during the impact. Since this context is rather aggressive to sensors and there was
10 no guarantee that the sensors would perform satisfactorily, redundant measurements were taken using different techniques. This redundancy aims at increasing the chance of obtaining data while testing and validating the measurement devices in this particular context.

The structure is instrumented with the aim of evaluating (i) the displacements, (ii)
15 the energy transfer and (iii) the damage to the structure. Stress measurements were not possible since the fill materials were coarse. As shown in Fig. 2, the measurement devices were placed in two vertical planes normal to the front facing: the first in the impact direction and the second one 2 m distant, respectively referred to as the "impact plane" and the "distant plane" in the following. In the impact plane, displacements are
20 assumed to occur in this plane only for symmetry reasons, contrary to the distant plane where normal to the plane displacements are expected. The position of the sensors in the impact plane is depicted in Fig. 3.

Displacements within the embankment are measured using rod displacement sensors connected to six different points in the impact plane: three points at the front–
25 kernel interface and 3 at the kernel–levee interface, at three heights from the ground (1.5 m, 2.5 m and 3.5 m). The six displacement sensors are supported by a rigid steel beam at the rear of the levee.

Discussion Paper | Discussion Paper | Discussion Paper | Discussion Paper |

NHESSD

2, 491–533, 2014

Real-scale response of a protection embankment

S. Lambert et al.

Title Page

Abstract | Introduction

Conclusions | References

Tables | Figures

|◄ | ►|

◄ | ►

Back | Close

Full Screen / Esc

Printer-friendly Version

Interactive Discussion

Accelerometers placed within and on the structure allow monitoring the compression wave propagation and soil particle displacement. The piezoresistive technology was preferred to other accelerometer technologies based on previous impact experiments involving smaller impact energies on a smaller structure (Haza-Rozier et al., 2010; Heymann et al., 2010). In the impact plane, eight different points within the structure are equipped: six accelerometers at the same locations as the displacement sensor extremities and two others in the middle of the kernel, 0.5 m and 4 m above the ground. In the distant plane, accelerometers are positioned in five different points, in the middle of the kernel and at the kernel–levee interface. Depending on the expected displacement of the point considered, acceleration is measured in one, two or three directions. A total of 11 acceleration measurements concern the impact plane and nine concern the distant plane. For this purpose, uni-axial accelerometers (measuring range ±200 g, bandwidth 0–1.5 kHz) and tri-axial accelerometers (measuring range ±100 g, bandwidth 0–1 kHz) are used. Accelerometers are placed on PVC supports and protected from impact by a cap. The supports are fixed to the gabion mesh. In the following, data from the eight accelerometers designated in Fig. 4 will be presented. Data will be referred to using the accelerometer number (no. 1–4 and no. 5–8 in the impact plane and distant plane, resp.) and the measurement direction with respect to the global system of axis shown in Fig. 4.

Displacements within the levee along the vertical axis are measured with an automatic inclinometer placed 0.5 m beyond the levee–kernel interface in the impact plane. Another inclinometer is located in the distant plane, at the same distance from the kernel–levee interface.

All the experiments were filmed using a high-speed camera at the rate of 250 frames per second. The impact angle and the projectile incident velocity were determined and the impact energy was computed. Images during the impact were used to track the penetration of the projectile in the embankment but could not be used to compute its velocity and acceleration, because the frequency was too small to satisfactorily reproduce the rapid changes in acceleration.

A topographical survey was performed before and after each impact to monitor the external deformation of the structure, also giving the sensor's exact position during structure construction. Targets are fixed on the wire mesh of the front face, with a spatial frequency of 0.5 m and 1 m in the vicinity and 2 m away from the impact area, respectively. Changes in the levee's mechanical characteristics are evaluated based on tomography. Velocities of P waves and S waves are measured before and after each impact in order to highlight the possible changes in the levee compaction.

The projectile is equipped with a tri-axial capacitive accelerometer (± 200 g) placed at its centre of mass. As the projectile was free to rotate, the orientation of the accelerometer axis with respect to the embankment facing varied from one test to the other.

The data logger, with a synchronous acquisition on 24 channels at a 10 kHz frequency, records the data from all the accelerometers, in the projectile and in the sandwich wall. The automatic inclinometer and the displacement sensors have their own data loggers.

2.4 Data treatment and validation

The impact beginning is considered as the time reference for all the signals. All the collected signals are corrected from the offset and filtered. This is particularly important when accelerometers are placed in contact with the quarry limestone. Indeed, impact leads to stone displacement and crushing, resulting in very rapid force variations requiring signal smoothing (Lambert et al., 2009).

The projectile acceleration measurement is used to calculate the three components of the projectile velocity and displacement by successive time integrations. The kinetic energy of the projectile during the impact (KE) is calculated using the velocity norm. The displacement of the projectile from the impact beginning, $U(t)$, is calculated as the norm of the three components of the displacement. The penetration of the projectile in the embankment, normal to the vertical facing, is computed as the horizontal

component of the projectile displacement:

$$U_h(t) = \cos\alpha U(t) \qquad (1)$$

with α the incident angle of the projectile.

5 The so-called impact force is derived from the projectile deceleration using Newton's 2nd law. In order to compute a stress from this force, the surface considered is the interception between the embankment facing plane and the projectile (Fig. 5). The area of this surface is given by

$$S(t) = \pi \cdot r^2 \quad \text{with} \quad r = \sqrt{2 \cdot R \cdot U_h(t) - U_h(t)^2} \qquad (2)$$

with R the radius of the projectile and $U_h(t)$ its penetration in the embankment. This
10 area represents the projection of the real facing–projectile contact surface on the surface normal to the penetration direction. It is thought to be the most relevant for computing a stress value based on the force acting on the projectile (i.e. the impact force).

The validity of the measurements and derived values was checked by comparing data from different sensor types.

15 The penetration derived from acceleration measurements fit rather well with measurements from other methods (Fig. 6). A rather good agreement with displacement derived from the high-speed camera images was observed during impact ($U_h(t)$ vs. U-camera), as well as with the final indentation measured with topographical survey ($U_h(t)$ vs. U-topo). The accelerometer tended to slightly overestimate the acceleration,
20 because penetration derived from this measurement was less than with the camera. The agreement concerning the maximal penetration values was considered good because the difference was about 10 %.

In a similar way, displacements within the embankment derived from accelerometer measurements were in rather good agreement with data from displacement sensors
25 (e.g. Fig. 7). The difference was most often less than 10 %.

These comparisons validate the use of sensors in this context, and the method for integrating acceleration to obtain the displacement with time.

2.5 Experiments

The experiments consisted in submitting the structure to successive impacts varying the projectile pre-impact velocity. Four levels of translational kinetic energy were targeted: 200 kJ, 500 kJ, 1000 kJ and 2000 kJ. The real impact conditions are detailed in
5 Table 1.

Structural damage was observed during the test series. It was limited for low impact energies: the 210 kJ impact only led to a facing deformation, with minor stone breakage. With increasing energy, the deformation of the facing increased and progressively advanced to the rest of the structure. The 2200 kJ impact led to substantial facing
10 damage with destroyed wire mesh and generalized stone crushing, but the structure remained stable after removing the projectile.

The structure facing was repaired before conducting tests 3 and 4 according to two techniques. When the impact resulted in severe damage of the front-facing geocells (test 2, with a 1000 kJ impact) the geocells involved were removed and replaced with
15 identical ones. Removing the front geocells was possible without any structural collapse risk due to the presence of internal connecting wires in the kernel geocells. In case of moderate damage, such as after test 3, repair consisted in placing a wire mesh patch on the front facing, connecting it to the front wall geocells with wires and backfilling it with crushed quarry limestone. These repairs were assumed to restore the structure's
20 ability to withstand the impact but obviously also slightly modified its characteristics.

In spite of the precautions taken for their installation, some sensors and sensor wires were damaged by the successive impacts. More precisely, large and non-uniform displacements that occurred in the structure led to tension in wires, resulting in excessive noise or absence of signal on some accelerometers. Shocks within the structure dam-
25 aged some sensors mainly in contact with stones. This is particularly true for the last test, at the 2200 kJ impact energy, and to a lesser extent for test 3. Due to a dysfunction of the main data logger, no data are available for test 2.

S. Lambert et al.

Title Page

Abstract | Introduction

Conclusions | References

Tables | Figures

|◀ | ▶|

◀ | ▶

Back | Close

Full Screen / Esc

Printer-friendly Version

Interactive Discussion

3 Analysis of experimental results

The structure's response is investigated in detail based in the first experiment, with a 210 kJ kinetic energy, given that all data were available. The analysis focuses on the accelerometer data. Then the results concerning the response of the structure to increasing impact energy are presented.

3.1 The structure's response to the 210 kJ impact

The impact of the projectile on the structure facing was characterised by a triangular and non-symmetrical projectile acceleration, with a peak value of $150\,\mathrm{m\,s^{-2}}$ (Fig. 8a). This maximum was reached 20 ms after the impact beginning and corresponds to an impact force of about 1000 kN. The total impact duration was about 200 ms. The projectile kinetic energy rapidly decreased: it was less than half its initial value 40 ms after the impact beginning. Comparison with displacements depicted in Fig. 6 shows that the penetration at the acceleration peak time was 0.15 m and that the maximum penetration was reached long after this acceleration peak (150 ms vs. 20 ms resp.).

The contact surface between the projectile and the structure facing increased with the projectile penetration (Fig. 8b) and the stress curve exhibited differences with the projectile acceleration curve: a steeper increase (7 ms), a well-marked quasi-plateau for almost 8 ms followed by a sharp decrease until 40 ms. The maximum stress reached exceeded 1500 kPa, enough to generate stone crushing as locally observed after the test.

The structure's response to this loading is investigated in detail by using measurements from sensors within the embankment. Figure 9 shows acceleration, velocity and displacement along the y-axis direction of two points close to the impact axis direction, namely A_1 and A_3 located 2.5 m from the ground at the front–kernel and kernel–levee interfaces, respectively. Between the two acceleration peaks, a time lag of about 30 ms is observed together with an amplitude reduction by a factor of 8.

Five different phases can be distinguished considering the three graphs plotted in Fig. 9. Phase I corresponds to a compression phase of the kernel. It lasts from 20 to 40 ms and follows the stress plateau observed in Fig. 8. During this phase, the first interface (i.e. A_1) experiences a rapid acceleration, contrary to the second interface (i.e. A_3). This difference in acceleration results in a difference in velocity and displacement (Fig. 9b and c). Phase II starts from the time the second interface begins moving (40 ms). From this time, the kernel is progressively shifted in the impact direction. Compression still develops due to the difference in velocity between the two interfaces. The maximal kernel thickness reduction is 120 mm, reached at the end of this phase (100 ms). During the next phase (III, 100–145 ms), both velocities decrease but the kernel progressively expands due to the difference in interface velocity. This expansion lasts until the end of the impact. During phase IV (145–175 ms), the two interfaces move in opposite directions. Finally, in the last phase (V) both velocities are negative, revealing a global kernel displacement in the direction opposite the impact direction (Fig. 9c).

At the end of the impact, the kernel almost returns to its initial position with a thickness increased by about 25 mm. By contrast, comparison of the projectile's penetration curve with the displacement curve of sensor A_1 reveals that the residual front-facing thickness reduction is more than 250 mm. These results show that the deformation of the structure is mainly localized on the front-facing layer of the sandwich and that the kernel has a high elastic recovery.

The rather high displacement of point A_3 certainly results from the fact that the levee soil was poorly compacted close to the kernel, as mentioned above. Nevertheless, displacements at the kernel–levee interface rapidly decrease with the distance from the impact axis direction (Fig. 10). The maximal displacement along the y-axis direction 1 m above and 1 m below A_3 in the impact plane does not exceed 44 mm and 30 mm, respectively (sensors A_4 and A_2). In the distant plane, the maximal displacement is less than 10 mm (sensors A_7 and A_8).

Title Page

Abstract | Introduction

Conclusions | References

Tables | Figures

|◄ | ►|

◄ | ►

Back | Close

Full Screen / Esc

Printer-friendly Version

Interactive Discussion

Figure 10 also shows the differences in displacement orientation from one sensor to the other. At the displacement peak, the displacement of sensor A_3 is mainly oriented along the y-axis, while it also occurs along z-axis for sensor A_4 located 1 m above, revealing a significant upward displacement of the latter. In the distant plane,
5   the displacement mainly occurs along the x-axis. More or less all sensors underwent a residual downward movement, revealing a small post-impact structure settlement.

The residual displacements along the y-axis are negative for sensors A_4, A_7 and A_8, suggesting that the structure globally moves opposite the impact direction. This displacement is more pronounced close to the crest (e.g. A_4 vs. A_2). The same trend
10   was observed within the levee above a height of 3 m from the ground (Fig. 11).

Similarly to what is observed for sensors A_7 and A_8 in the distant plane at the kernel–levee interface, sensors placed in the middle of the kernel in this same plane exhibit a significant residual displacement along the x-axis (Fig. 12). Considering the position of these sensors with respect to the impact point, this displacement is believed to partly
15   result from the lateral expansion of the kernel in the impact axis direction, which undergoes compression along the y-axis. The residual displacement along the x-axis of A_7 is smaller than that of A_6, both positioned 3.5 m from the ground (3 mm/14 mm). This is attributed to the geocell wire netting along the kernel–levee interface that counters the displacement after the load peak (sensor A_7).
20   Based on these measurements, a schematic analysis of displacements observed at the impact height (2 m above ground) over time can be proposed (Fig. 13). The second stage typically corresponds to the maximum projectile penetration. Each geocell deforms along the two directions, with compression in the impact direction (y axis) and dilation in the tangential direction (x axis). The latter mechanism is partly countered by
25   the internal connecting wires and by the wire netting at the vertical interfaces between the different layers. The deformation of the front facing does not concern the only impacted area. On the contrary, geocells around this area seem to be driven in the impact direction. This effect is attributed to the wire netting on the front facing that distributes the load to soil masses at a distance on both sides of the impacted area. As a con-

sequence, the mass involved in the structure's response is increased and the stress diffusion angle is also expected to be higher. Both these mechanisms have a beneficial effect on the structure's ability to withstand the impact. The third stage corresponds to the global structure reverse displacement. This mechanism is mainly attributed to the elasticity of the sand–tyre mixture (Lambert et al., 2009).

3.2 High-energy impact responses

The damage to the structure as well as the penetration increased with increasing projectile kinetic energy. As the structure halted the projectile without collapsing, it can be considered that the maximum impact energy remains below the nominal capacity of the structure (Fig. 14).

After the fourth test, the structure exhibited different main deformation patterns depending on the plane: compression in the impact plane and bending in the distant plane (Fig. 15). Cracks parallel to the kernel–levee interface were observed on the embankment crest between the kernel and the levee as well as about 1 m from this interface. Levee soil density changes were observed: bulking close to the kernel–levee interface as well as at a distance typically 2 m from this interface and compaction about 0.9 m from the interface, at a depth of 1–2 m from the crest.

The structure's response is first addressed in detail based on the displacements at the kernel–levee interface, which is an indirect but convenient estimator of the sandwich wall efficiency in reducing the stress on the levee.

The incremental displacement of sensors in the impact plane during impact tests 1, 3 and 4 is depicted in Fig. 16. The displacements strongly depend on the point considered and on the impact test. In the case of sensor 3, the deformation localization observed after test 1 vanished for the other tests. For sensors 2 and 4, respectively above and below the impact height, a clear increase trend from the first to the last test was observed for both the maximum and residual displacement values. This trend mainly results from the displacement along the y-axis, this value predominating over the two other components. By contrast, the upward displacement increased during the

test series and depending on the position of the sensor. At maximum, sensor A_4 moved by 160 mm and 80 mm along the y-axis and z-axis, respectively, during the last test.

The results globally reveal a change in the structure's response: while the first impact evidences strain concentration, the two other impacts reveal a tilting movement on the whole structure, with higher amplitude close to the crest.

The interface displacements, i.e. the displacements along the y-axis, were much smaller than the projectile penetration (Table 2). Maximum penetrations as large as 1 m were measured during tests 2 and 4. The residual penetration was typically 70 % the maximum penetration. By contrast, displacements measured at the kernel–levee interface were much lower, with residual values typically 10 % the projectile residual penetration. The maximum reverse displacement of the kernel–levee interface, i.e. in the direction opposite the impact direction, was 70 mm (test 4). This may result from the kernel layer elasticity rather than from a real soil levee displacement. The sensor was connected to the wire netting whose reverse displacement led to a void between the geocell and the levee (cracks, see Fig. 15).

3.3 Comparison with other structure types

The limited number of real-scale impact experiments that have been conducted investigated structures differing in their cross-sectional shape, construction materials and size (Lambert and Bourrier, 2013). Testing conditions also varied from one study to another in terms of projectile mass and velocity. Despite this variability, these experiments globally provide a valuable database for comparison with the results presented in this paper. For this purpose, a representative panel of experiments from Hearn et al. (1996), Yoshida (1999), Peila et al. (2000, 2007), Sung et al. (2008) and Maegawa et al. (2011) is considered. The considered experiments investigated an impact by a single projectile with a kinetic energy in the 50–2500 kJ range at the structure's mid-height approximately. The criterion for comparison is the residual projectile penetration, the only data recorded in all cases (Table 3).

For the lowest impact energies, the deformation of the front facing is similar for all cases (typically 300 mm for 200 kJ). Differences appear when increasing the projectile's kinetic energy. For impact energies around 1000 kJ, the maximum deformation measured on structures tested by Maegawa et al. (2011) was three times higher than that for cellular sandwich walls (our study). For impacts involving 2000 kJ kinetic energy projectiles, the latter type of structure performed similarly to structures tested by Peila et al. (2000, 2007) in terms of penetration.

Compared to the other structures, the width of the cellular embankment tested was significantly higher, with a possible positive influence on its ability to withstand the impact. The fact that the projectile was stopped before the kernel–levee interface started significantly moving suggests that only a limited volume of the levee was involved before the projectile was stopped. As a consequence, it may be suggested that the size of the levee could have been significantly reduced with only minor consequences on the embankment's ability to stop the projectile.

4 Discussion

On the whole, these results highlight several general trends regarding the response to localized impact of an embankment and its interaction with the projectile.

During the impact, the kinetic energy of the projectile is transferred to the embankment via the compression wave. It has been shown that the compression wave progressively travels from the impact point to the entire structure, within a cone. Its amplitude decreases due to both geometrical and material attenuations (Semblat and Luong, 1999; Ronco et al., 2009). The wave field can be considered spherical and the propagation direction radial from the impact point if the medium is isotropic and large enough. This compression wave results in a local increase in strain energy in the granular media, leading to plastic strain when in excess with respect to the mechanical characteristics of the material crossed. For instance, crushing of stones contained in the facing geocells and compaction in the levee have been shown in this study. More-

over, the rather large deformations of kernel geocells also suggest plastic strain in this layer. The compression wave also progressively leads to an increase in kinetic energy. Basically, each elementary volume of the structure exposed to an unbalanced force tends to be shifted in the wave propagation direction. Its displacement is countered by the neighbouring elementary volume in the wave propagation direction, which acts as a buttress. This buttress effect depends on the neighbouring volume unit mass, mechanical characteristics and average stress. This explains why the upward movement at the kernel–levee interface displacements is higher above the projectile penetration axis, i.e. close to the crest. This phenomenon has been mentioned previously (Peila et al., 2007; Soudé et al., 2013; Hofmann et al., 2013). It results from the fact that the crest is a free boundary and that the weight of material above decreases, both resulting in a decrease in the buttress effect. The same mechanism explains the difference in soil levee characteristic changes observed from one point to another. Both the crack observed on the crest, 2 m from the kernel–levee interface and the decrease in seismic velocity observed more or less at the same distance within the levee core occurred due to an insufficient buttress effect. More precisely, when approaching the facing opposite the impacted facing, the compression wave resulted in increasing soil displacement. By contrast, at a distance of 1.5 m from the kernel–levee interface in the levee core, the compression wave increased soil compaction because the buttress effect was sufficient and reduced the soil displacement.

During the first test, with a 210 kJ impact, the projectile was stopped in less than 200 ms and the maximum impact force was reached at 20 ms. The projectile kinetic energy loss was rapid: 50 % and 90 % in 35 ms and 95 ms, respectively. This contrasts with the characteristic time related to the structure's response. For example, the kernel–levee interface significantly moved starting at 50 ms and reached its maximum displacement at about 190 ms. This shows that the interaction between the projectile and the embankment mainly involves a fraction of the structure, typically 2 m away from the impact point. Likewise, the maximum impact force that is often used for the design of embankments is related to an even more limited fraction of the structure as it is

Real-scale response of a protection embankment

S. Lambert et al.

reached at the very beginning of the impact. This impact force may not be relevant for evaluating the load transmitted and thus displacement far away from the impact point.

These results suggest that the mechanical characteristics of the materials near the front facing govern the projectile–structure interaction and consequently the impact force, with consequences on the stress transmitted within the structure, while the characteristics of the whole structure govern its response and ability in surviving the impact load. More generally, the description of the structure's response given in this study suggests that relevant design methods should be able to account for both the projectile–structure–facing interaction, on one side, and on the so-called buttress effect of the rest of the structure.

One of the key issues in assessing the response of rockfall protection embankments to impact is energy dissipation. Dissipation may result from three main mechanisms generating plastic strain: compaction, friction and crushing. The contribution over time of each of these mechanisms depends on the mechanical characteristics of the fill materials, on the distance to the impact point and on the impact energy (Lambert and Bourrier, 2013). According to numerical simulation results, compaction has been shown to predominate in embankments made up of fine granular materials for high-energy impacts (Ronco et al., 2009). However, measuring the different energy dissipation terms over time is not possible through experiments, and, in this specific case, estimating the dissipation by computing the kinetic and strain energy is tricky. The velocity field over the whole structure is too complex to estimate the kinetic energy precisely and it is difficult to compute strain energy in coarse materials as well as in the sand–tyre mixture undergoing significant strain and displacements. Finally, the propagation of the compression wave in the structure is not as simple as in infinite and isotropic media. Although not evidenced by the measurements, it can be stated that mechanisms such as scattering and reflection occur, with significant influence on the wave field and consequently on the displacement field. Leaving aside the question of tracking energy in the structure, the discussion mainly focuses on the advantages of sandwich structures based on the interpretation of the measurements.

The choice of different fill materials for the facing and kernel geocells aims at improving the efficiency of the sandwich by reducing the stress transmitted to the levee. Two ideas support this concept. First, deformation within the structure induces an increase in impact duration, resulting in a decrease in the stress transmitted. Indeed, it was shown that the stress transmitted by a sandwich structure was significantly reduced when decreasing the modulus of the kernel material (Bourrier et al., 2011). Second, deformation should preferably result from irreversible mechanisms leading to energy dissipation. As shown in a previous experimental study (Lambert et al., 2009), crushing is a fundamental phenomenon in the impact response of geocells filled with stones. First, crushing dissipates energy and, second, it limits the stress to a threshold, which depends on the size and crushing resistance of the stones. This limitation results in greater penetration of the projectile and a longer-lasting impact. In addition, at the structure scale, crushing leads to the quasi-plateau observed on the contact surface stress curve (Fig. 8). The same study shows that geocells filled with a sand–tyre mixture exhibit a smaller modulus and a smaller residual penetration and that the energy restitution to the projectile was higher than with geocells filled with stones. This difference stems from the progressive compaction of this finer fill material with increasing geocell deformation, its elastic properties and its interaction with the geocell envelope (Lambert et al., 2011). This is consistent with observations at the structure scale where high elastic recovery of the kernel was observed.

The difference in the compression response of the two layers, in terms of thickness reduction, thus directly results from the characteristics of the fill material.

5   Conclusion

In order to assess the response of cellular sandwich protection embankments to rockfall impacts, real-scale impact experiments were conducted using a projectile with translational kinetic energies up to 2200 kJ. The structure was made up of a two-layer sandwich wall consisting of gabion cages filled with either stones or a sand–scrapped-

tyre mixture, leaned against a compacted soil levee. For the first time, the impacted structure was instrumented with accelerometers, displacement sensors and inclinometers.

The experiments provided highly valuable real-time data for understanding the response of these structures. Comparison of the data from different sensor types was necessary for validation purposes. Nevertheless, this measuring context appeared highly detrimental to sensors, in particular due to the repetition of impacts.

Crushing of the coarse materials comprising the front-facing layer dissipates energy and attenuates the stress on the second layer. The sand–tyre mixture exhibits elasticity that allows the second layer of the sandwich to restore its dimensions after impact. The wire netting distributes the load within the structure, while facilitating the structure post-impact repair.

The experiments prove the structure to be efficient for impact energies of at least 2200 kJ. The levee dimensions may be reduced without altering this ability. Moreover, the sandwich technology may be an efficient way to improve the efficiency of existing embankments. A sandwich wall leaned against an existing embankment will increase its ability to withstand high-energy impacts.

Finally, the set of collected data are of great interest for calibrating and validating numerical tools, and in particular the models based on DEM, FEM and DEM/FEM coupling whose development has been initiated within this research project (Nicot et al., 2007; Breugnot et al., 2010).

References

Aminata, D., Yashima, A., Sawada, K., and Sung, E.: New protection wall against rockfall using a ductile cast iron panel, Journal of Natural Disaster Science, 30, 25–33, 2008.

Bertrand, D., Nicot, F., Gotteland, P., and Lambert, S.: Modelling a geo-composite geocell using discrete analysis, Comput. Geotech., 32, 564–577, 2005.

Blovsky, S.: Bewehrungsmöglichkeiten mit Geokunststoffen, PhD Dissertation,. Technische Universität Wien, Austria, 2002.

5 Bourrier, F., Lambert, S., Heymann, A., Gotteland, P., and Nicot, F.: How multi-scale approaches can benefit cellular structure design, Can. Geotech. J., 48, 1803–1816, doi:10.1139/t11-072, 2011.

Breugnot, A., Gotteland, P., and Villard, P.: Numerical modelling of impacts on granular materials with a combined discrete-continuum approach, in: Proceedings of the 7th European

10 conference on Numerical Methods in Geotechnical Engineering Trondheim, Norway, 2–4 June, 477–482, 2010.

Burroughs, D. K., Henson, H. H., and Jiang, S. S.: Full scale geotextile rock barrier wall testing, analysis and prediction, in: Proceedings of Geosynthetics '93, Vancouver, Canada, 30 March–1 April, 959–970, 1993.

15 Dimnet, E., Haza-Rozier, E., Vinceslas, G., Leon, R., and Hernandez, G.: Experimental and numerical study of a shock-absorbing structure, Acta Mech., 224, 3037–3055, 2013.

Gotteland, P., Lambert, S., and Salot, C.: Investigating the strength characteristics of tyre chips–sand mixtures for geo-cellular structure engineering, in: Proceedings of the International Workshop on Scrap Tire Derived Geomaterials – Opportunities and Challenges, Yokosuka,

20 Japan, 23–24 March 2007, 351–361, 2008.

Haza-Rozier, E., Reiffsteck, P., Vinceslas, G., Lambert, S., Heymann, A., Gotteland, P., and Douaillat, M.: Tests on shock-absorber structures on a swinging impact site, in: Proceedings of Journées nationales de géotechnique et de géologie de l'ingénieur, Grenoble, France, 7–9 July, 657–664, 2010.

25 Hearn, G., Barrett, R. K., and Henson, H. H.: Development of effective rockfall barriers, J. Transp. Eng.-ASCE, 121, 507–516, 1995.

Hearn, G., Barrett, R. K., and Henson, H. H.: Testing and modelling of two rockfall barriers, Transport. Res. Rec., 1504, 1–11, 1996.

Hennebert, P., Lambert, S., Fouillen, F., and Charrasse, B.: Assessing the environmental impact

30 of shredded tires as embankment fill material, Can. Geotech. J., accepted, doi:10.1139/cgj-2013-0194, 2014.

Heymann, A., Lambert, S., Haza-Rozier, E., Vinceslas, G., and Gotteland, P.: An experimental comparison of real–scale rockfall protection sandwich structures, in: Proceedings of the 11th conference on Structures under shock and impact, Tallinn, Estonia, 28–30 July, 15–26, 2010.

Heymann, A., Collombet, M., Lambert, S., and Gotteland, P.: Use of external testing methods to assess damage on rockfall protection structures, Appl. Mech. Mater., 82, 704–709, 2011.

Hofmann, R., Vollmert, L., and Mölk, M.: Rockfall-protection embankments – design concept and construction details, in: Proceedings of 18th International Conference on Soil Mechanics and Geotechnical Engineering, Paris, France, 2–6 September, 3107–3110, 2013.

Lambert, S. and Bourrier, F.: Design of rockfall protection embankments: a review, Eng. Geol., 154, 77–88, doi:10.1016/j.enggeo.2012.12.012, 2013.

Lambert, S., Gotteland, P., and Nicot, F.: Experimental study of the impact response of geocells as components of rockfall protection embankments, Nat. Hazards Earth Syst. Sci., 9, 459–467, doi:10.5194/nhess-9-459-2009, 2009.

Lambert, S., Nicot, F., and Gotteland, P.: Uniaxial compressive behavior of scrapped-tire and sand-filled wire netted geocell with a geotextile envelope, Geotext. Geomembranes, 29, 483–490, doi:10.1016/j.geotexmem.2011.04.001, 2011.

Lambert, S., Bourrier, F., and Toe, D.: Improving three-dimensional rockfall trajectory simulation codes for assessing the efficiency of protective embankments, Int. J. Rock Mech. Min., 60, 26–36, doi:10.1016/j.ijrmms.2012.12.029, 2013.

Lee, H. J. and Roh, H. S.: The use of recycled tire chips to minimize dynamic earth pressure during compaction of backfill, Constr. Build. Mater., 21, 1016–1026, 2007.

Maegawa, K., Tajima, T., Yokota, T., and Tohda, M.: Experiments on rockfall protection embankments with geogrids and cushions, International Journal of GEOMATE, 1, 19–24, 2011.

Nicot, F., Gotteland, P., Bertrand, D., and Lambert, S.: Multi-scale approach to geo-composite cellular structures subjected to impact, Int. J. Numer. Anal. Met., 31, 1477–1515, 2007.

Peila, D.: Ground reinforced embankments for rockfall protection: from real scale tests to numerical modelling, in: Rockfall Engineering, edited by: Lambert, S. and Nicot, F., John Wiley & Sons, ISTE ltd, New York, London, 393–426, 2011.

Peila, D., Castiglia, C., Oggeri, C., Guasti, G., Recalcati, P., and Sassudelli, F.: Full scale tests on geogrid reinforced embankments for rock fall protection, in: Proceedings of the 2nd European Geosynthetics Conference and Exhibition, Bologna, Italy, 15–18 October, 317–322, 2000.

Real-scale response of a protection embankment

S. Lambert et al.

Peila, D., Oggeri, C., and Castiglia, C.: Ground reinforced embankments for rockfall protection: design and evaluation of full scale tests, Landslides, 4, 255–265, 2007.

Pichler, B., Hellmich, C., and Mang, H. A.: Impact of rocks onto gravel – design and evaluation experiments, Int. J. Impact Eng., 31, 559–578, 2005.

Ronco, C., Oggeri, C., and Peila, D.: Design of reinforced ground embankments used for rockfall protection, Nat. Hazards Earth Syst. Sci., 9, 1189–1199, doi:10.5194/nhess-9-1189-2009, 2009.

Semblat, J.-F. and Luong, M. P.: Wave propagation through soils in centrifuge testing, J. Earthq. Eng., 2, 147–171, 1998.

Soudé, M., Chevalier, B., Grédiac, M., Talon, A., and Gourvès, R.: Experimental and numerical investigation of the response of geocell-reinforced walls to horizontal localized impact, Geotext. Geomembranes, 39, 39–50, 2013.

Sung, E., Yashima, A., Aminata, D., Sugimori, K., Sawada, K., Inoue, S., and Nishida, Y.: Numerical assessment of performance of protecting wall against rockfall, in: Proceedings of the 5th International Symposium on Earth Reinforcement, Fukuoka, Japan, 14–16 November 2007, 861–867, 2008.

Yoshida, H.: Recent experimental studies on rockfall control in Japan, in: Proceedings of the Joint Japan–Swiss scientific seminar on impact by rock falls and design of protection structures, Kanazawa, Japan, 4–7 October, 69–78, 1999.

Zornberg, J. G., Cabral, A. R., and Viratjandr, C.: Behaviour of tire shred-sand mixtures, Can. Geotech. J., 41, 227–241, 2004.

Real-scale response of a protection embankment

S. Lambert et al.

Title Page

Abstract	Introduction
Conclusions	References
Tables	Figures

|◀ | ▶|

◀ | ▶

Back | Close

Full Screen / Esc

Printer-friendly Version

Interactive Discussion

Table 1. Impact conditions.

Test #	Kinetic energy (kJ)	Velocity ($m\,s^{-1}$)	Incident angle (°)	Impact height (m)
1	210	8	18	1.8
2	1040	18	19	1.7
3	540	13	26	2.1
4	2200	26	24	2.1

Title Page

Abstract   Introduction

Conclusions   References

Tables   Figures

◄   ►

Back   Close

Full Screen / Esc

Printer-friendly Version

Interactive Discussion

Table 2. Sandwich structure deformation at the impact height.

Test #	Kinetic energy (kJ)	Projectile penetration		Kernel–Levee interface displacement	
		Maximum (mm)	Residual (mm)	Maximum (mm)	Residual (mm)
1	210	500	335	104	52
2	1040	980	730	na	na
3	540	670	420	73	10
4	2200	1010	710	124	55

Table 3. Comparison with previous real-scale experiments with similar impact conditions (NM: not measurable).

Authors	Embankment		Projectile kinetic energy (kJ)	Penetration (mm)
	Height (m)	Width (crest/base) (m)		
Aminata et al. (2008)	2	1.5/2.25	56	340
Yoshida (1999)	4	4.3/5.3	181	295
This study	4	3.5/9	210	335
Burroughs et al. (1993)	3.1	1.8/1.8	387	300
Maegawa et al. (2011)	4.2	2.2/4.3	697	824
This study	4	4.5/9	540	420
Burroughs et al. (1993)	3.1	1.8/1.8	1010	600
Maegawa et al. (2011)	4.2	2.2/4.3	1243	1560
This study	4	4.5/9	1040	730
Yoshida (1999)	4	3.3/5.3	2263	N.M.
Peila et al. (2000, 2007)	4.2	0.9/5	2500	600
Burroughs et al. (1993)	3.1	1.8/1.8	1400	900
Maegawa et al. (2011)	4.2	2.2/4.3	2037	1730
This study	4	4.5/9	2200	710

Fig. 1. View of the tested embankment, showing the sandwich wall leaned against the levee and the hanging projectile.
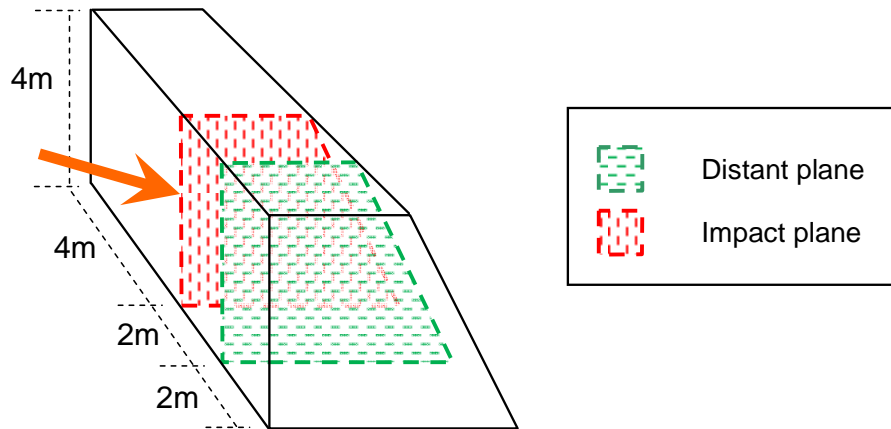
Fig. 2. Sensors within the structure were placed in two vertical planes: in the impact direction and 2 m aside.

Fig. 3. Cross section of the tested structure in the impact plane and measuring devices.
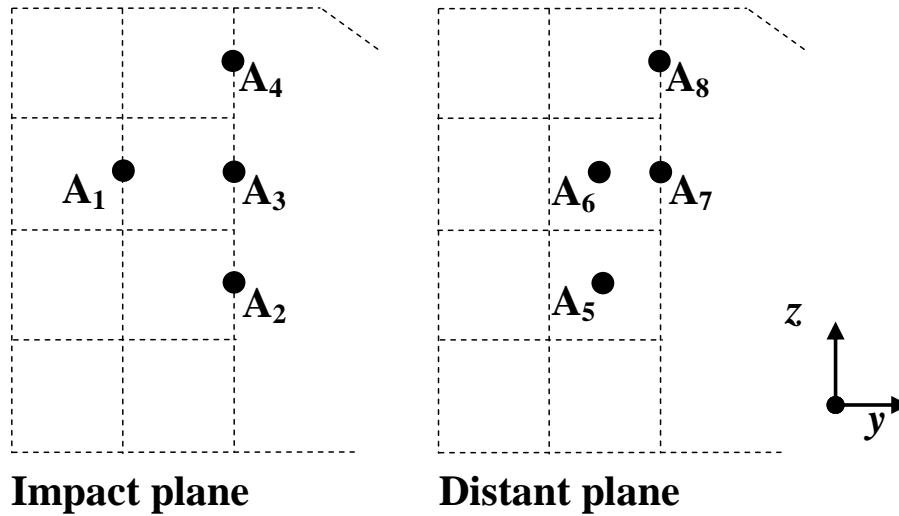
Fig. 4. Accelerometers considered in this study.
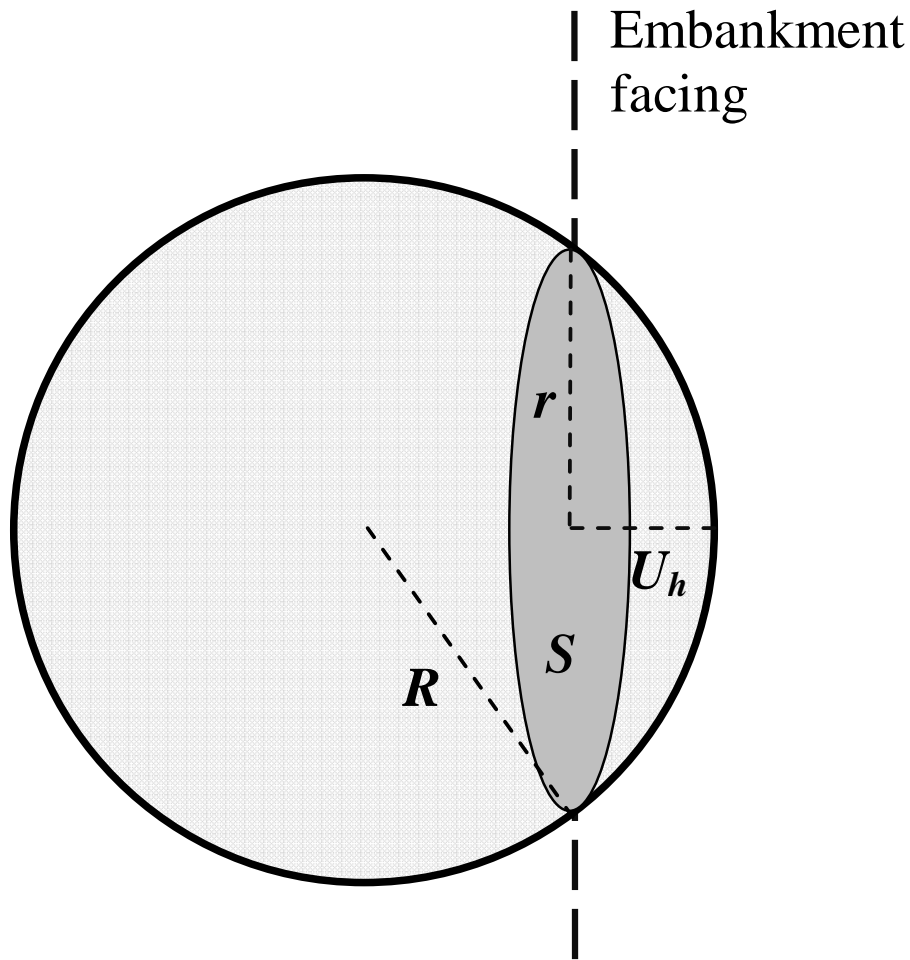
Fig. 5. Definition of the contact surface between the projectile and the embankment.

Title Page

Abstract · Introduction

Conclusions · References

Tables · Figures

|◄ · ►|

◄ · ►

Back · Close

Full Screen / Esc

Printer-friendly Version

Interactive Discussion
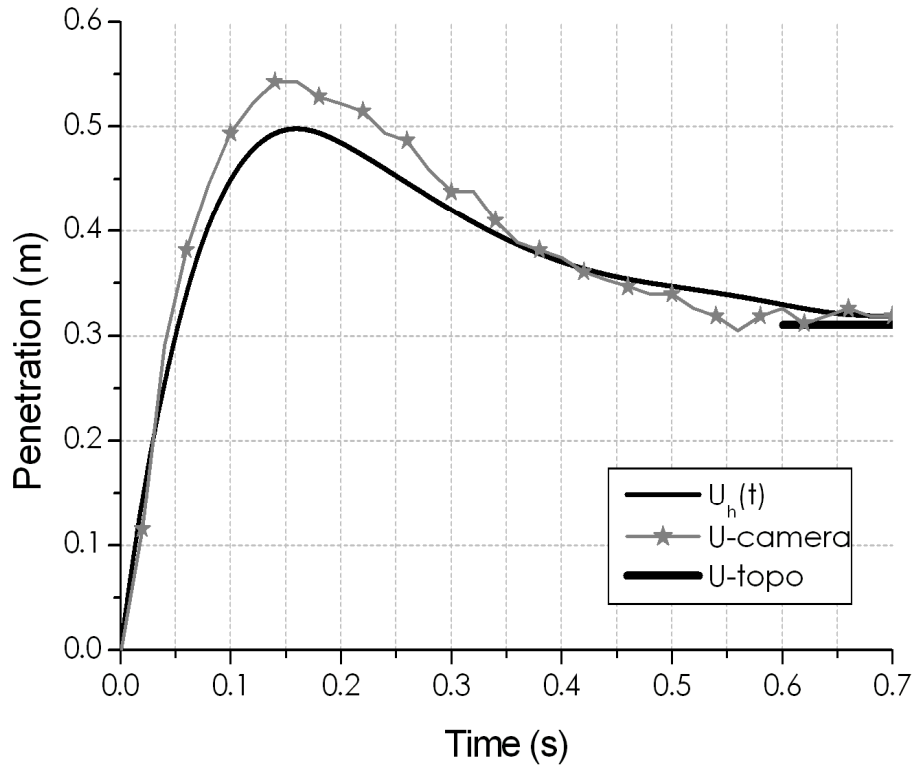
Fig. 6. Comparison of the different penetration estimates (210-kJ impact test).
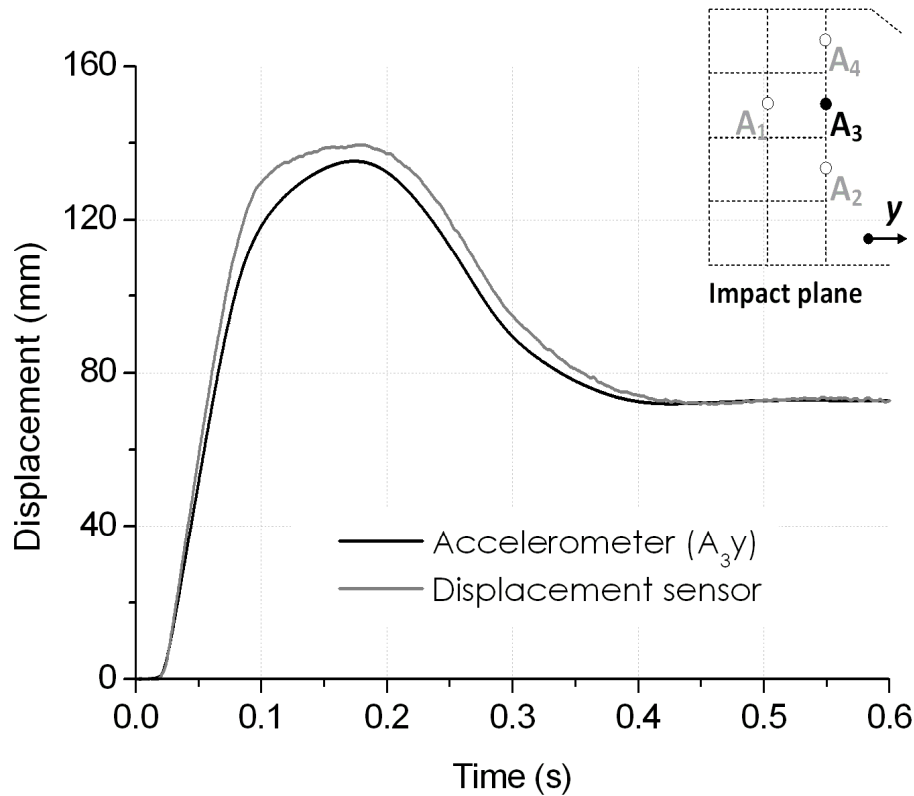
Fig. 7. Comparison of the horizontal displacement 3.5 m from the ground at the kernel–levee interface, based on accelerometer and displacement sensor data (2200-kJ impact test).
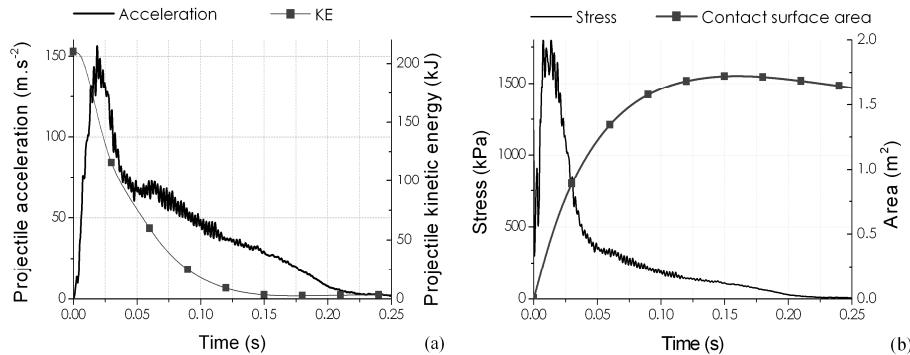
Fig. 8. (a) Acceleration and kinetic energy of the projectile and **(b)** projectile/embankment contact surface and stress at the structure's front face during the 210-kJ impact test.

Full Screen / Esc

Printer-friendly Version

Interactive Discussion
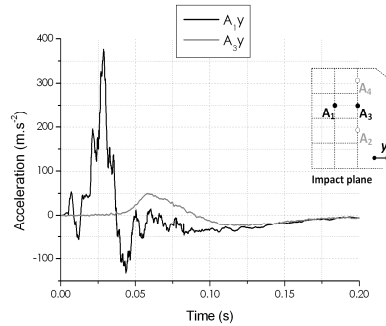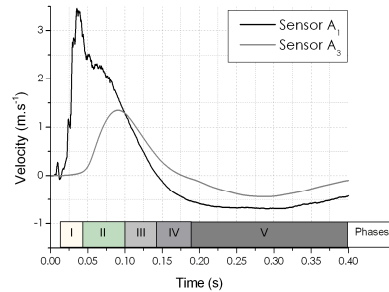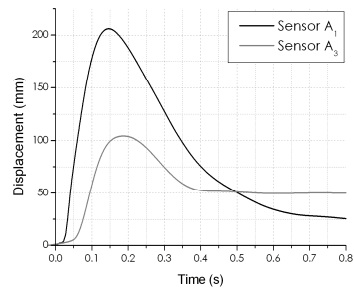
Fig. 9. Time evolution of acceleration, velocity and displacement along the y-axis direction at the front–kernel interface (A_5) and at the kernel–levee interface (A_6) in the impact plane.
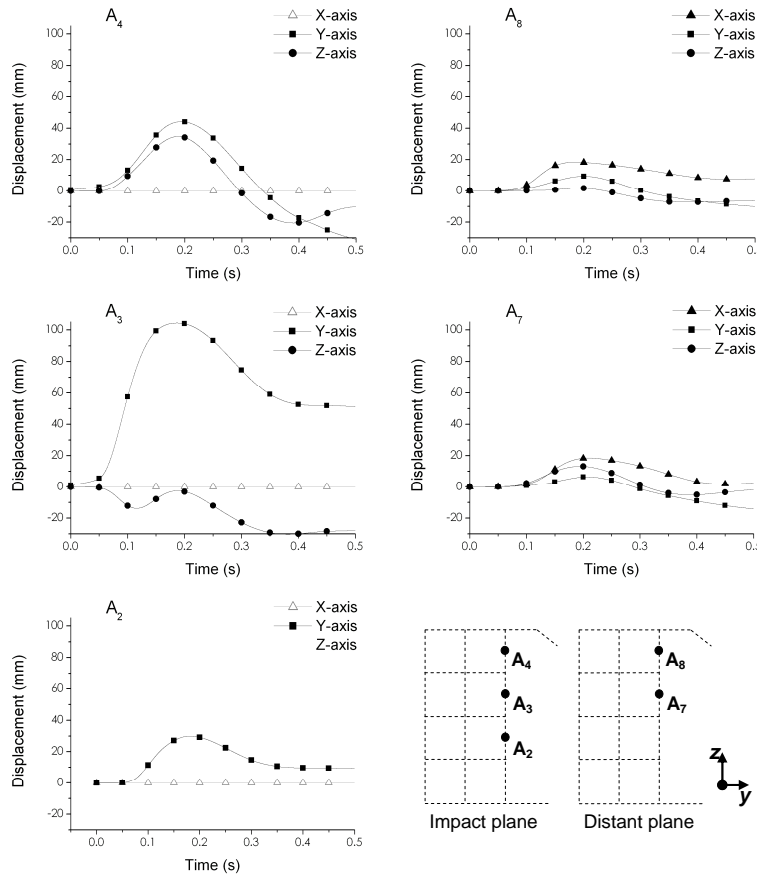
Fig. 10. Displacement of the five sensors placed at the kernel–levee interface: A_2, A_3, and A_4 in the impact plane, A_7 and A_8 in the distant plane. Open symbol curves display assumed values.
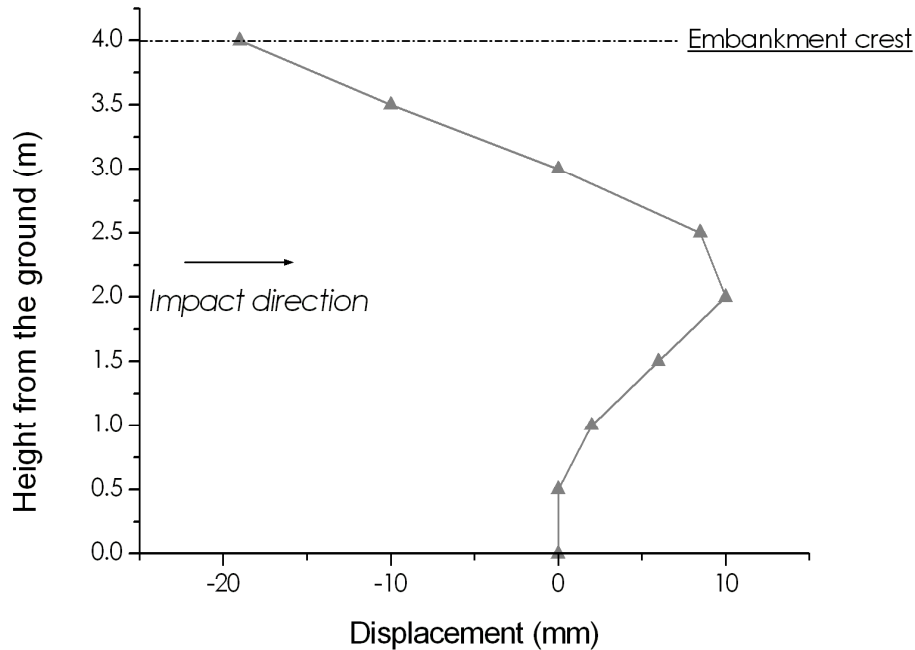
Fig. 11. Displacements measured with the inclinometer within the levee, 0.50 m from the kernel–levee interface.

Title Page

Abstract | Introduction

Conclusions | References

Tables | Figures

◀ | ▶|

◀ | ▶

Back | Close

Full Screen / Esc

Printer-friendly Version

Interactive Discussion
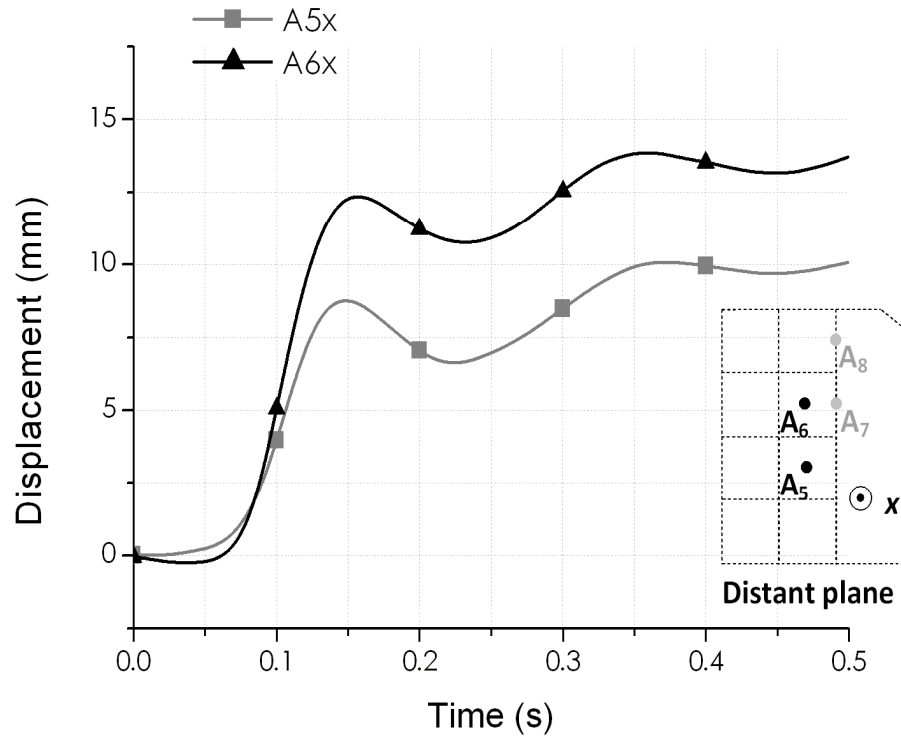
Fig. 12. Displacements in the middle of the kernel, in the distant plane, along the x-axis.

Title Page

Abstract | Introduction

Conclusions | References

Tables | Figures

|◄ | ►|

◄ | ►

Back | Close

Full Screen / Esc

Printer-friendly Version

Interactive Discussion
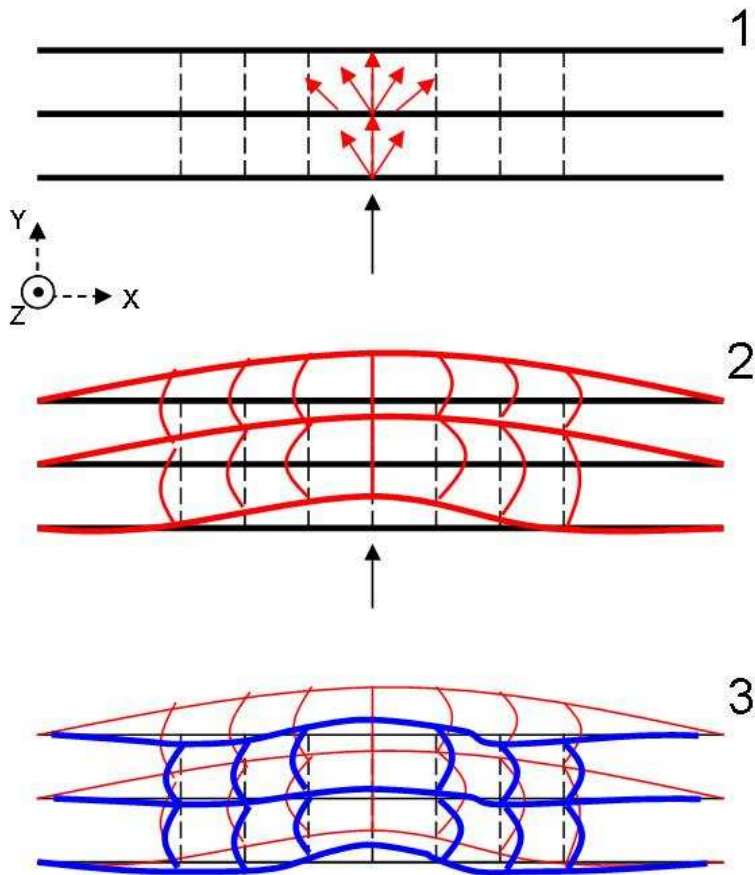
Fig. 13. Schematic representation of the deformation of the sandwich wall at the impact height (2 m above the ground): 1. beginning of impact, 2. maximum deformation stage, 3. residual deformation.
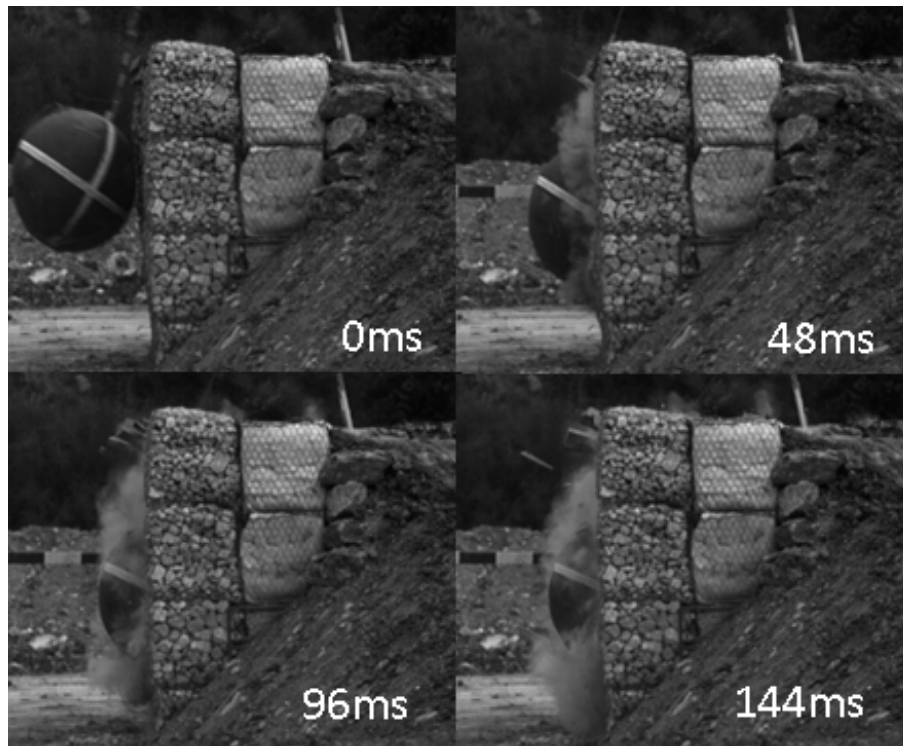
Fig. 14. High-speed camera images during the 4th impact test (2200 kJ).

Title Page

Abstract | Introduction

Conclusions | References

Tables | Figures

I◀ | ▶I

◀ | ▶

Back | Close

Full Screen / Esc

Printer-friendly Version

Interactive Discussion
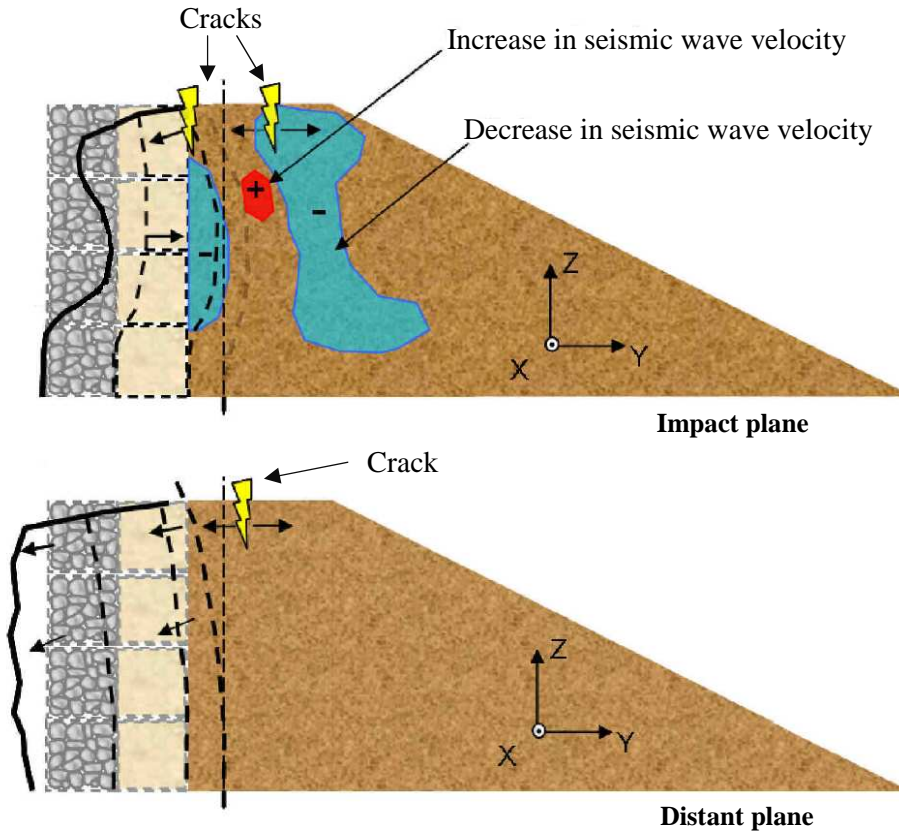
Fig. 15. After the fourth impact, the sandwich wall exhibited a different deformation pattern from one plane to the other. Cracks, compaction and bulking were observed in the levee.
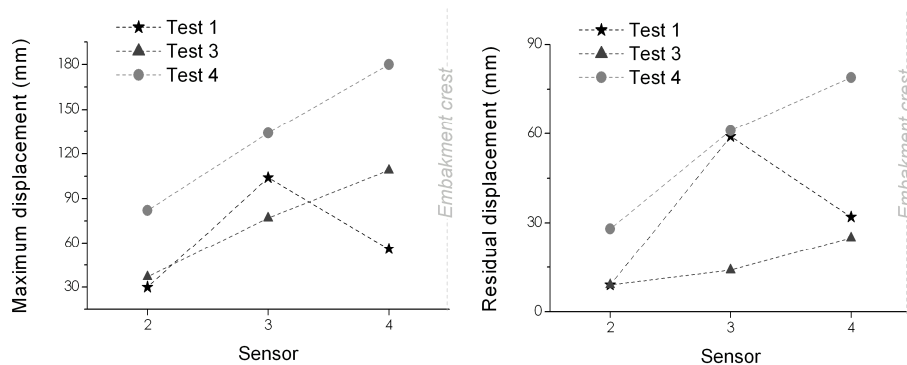
Fig. 16. Maximum and residual incremental displacements at the kernel–levee interface in the impact plane after each impact (sensors A_2, A_3 and A_4).

Title Page

Abstract · Introduction

Conclusions · References

Tables · Figures

|◄ · ►|

◄ · ►

Back · Close

Full Screen / Esc

Printer-friendly Version

Interactive Discussion